LAWRENCE
LIVERMORE
NATIONAL
LABORATORY

LLNL-CONF-649929

Experimental Determination of Chlorite Kinetics at Geothermal Conditions

M. M. Smith, S. A. Carroll

February 14, 2014

Stanford Geothermal Workshop
Stanford, CA, United States
January 24, 2014 through January 26, 2014

Disclaimer

PROCEEDINGS, Thirty-Ninth Workshop on Geothermal Reservoir Engineering
Stanford University, Stanford, California, February 24-26, 2014
SGP-TR-202

Experimental Determination of Chlorite Kinetics at Geothermal Conditions

Megan M. Smith and Susan A. Carroll

Lawrence Livermore National Laboratory; 7000 East Avenue, L-231; Livermore, CA, 94550 USA

megan@llnl.gov

Keywords: chlorite, mineral kinetics, geothermal geochemistry

ABSTRACT

Phyllosilicates such as clays and other sheet silicates are ubiquitous in geothermal environments, and are often assumed to react quickly when unequilibrated fluids are introduced to these systems. Rapid reaction of these phases may contribute to scaling reactions or alteration along fracture surfaces which can affect resource permeability; thus, knowledge of the reaction kinetics for these minerals is useful in modeling long-term reservoir performance. A suite of experiments was performed to develop a kinetic rate law for the dissolution of chlorite, $(Mg,Al,Fe)_{12}(Si,Al)_8O_{20}(OH)_{16}$, which is commonly noted in many geothermal host rocks as either a primary mineral or alteration product. We find that over temperatures of 100-275 °C, pH levels of 3-10, and even in the presence of dissolved carbon dioxide, the dissolution of chlorite is relatively slow compared to other common silicate minerals for which higher-temperature data are available (e.g., quartz, feldspars). This finding conflicts with a previously reported high activation energy for this reaction (Palandri and Kharaka, 2004), but is corroborated by comparison of our experimental data with two other relatively recent datasets collected at lower temperatures (Lowson et al., 2007; Black and Haese, 2014). The combined treatment of these data results in a kinetic rate equation that should be easily incorporated into most existing reactive transport codes for use in prediction of rock-water interactions in engineered geothermal systems.

1. INTRODUCTION

Development of engineered geothermal energy systems through the reactivation of fractures in deep hot rocks requires sustained permeability for about 30 years. Chemical reactions pose an important but poorly understood threat to the long-term success of enhanced geothermal systems (EGS), because critical kinetic data for fracture minerals at EGS target temperatures necessary to fully assess the risk are lacking. The poor understanding on the impact of rock-water interactions on fracture permeability is seen by the variable results from experimental laboratory studies on fractured rock cores. Some data suggest that chemical reactions can significantly reduce fracture permeability even at temperatures much lower than EGS target zones (200 to 400°C) (Polak et al, 2003; Carlson et al, 2005; Viani et al, 2005; Yasuhara et al, 2006, 2011; Yasuhara and Elsworth, 2008), while others in CO_2-rich environments show an increase in fracture permeability (Smith et al., 2013a). It is important to sort out the role of chemistry on EGS permeability, because reductions in fracture permeability will negatively affect heat transfer, possibly rendering the EGS system uneconomic. In principle the role of geochemistry could be assessed through modeling, unfortunately, kinetic data and rate equations are lacking for fracture filling minerals at EGS temperatures (200 to 400°C) and are rare even to 100°C (Cama et al, 2000; Brandt et al., 2003; Gustaffson & Puidomenech, 2003; Kohler et al., 2003; Carroll and Knauss, 2005; Lowson et al., 2005, 2007; Smith et al., 2013b). Use of the rates extrapolated from low temperature may overpredict dissolution by up to 10,000 times at typical EGS temperatures, leading to poor estimates of the true impact of geochemical alteration on EGS permeability (Smith et al., 2013b).

We address this need by measuring dissolution rates and deriving rate equations for fracture minerals identified in shear stimulation zones at EGS demonstration sites. The resulting rate equations can be directly incorporated into larger scale reactive transport simulations to assess the impact of geochemical reactions on shear zone permeability. Here we report 20 new chlorite dissolution rates measured from pH 3 to 10 and 100 to 275°C. These new rate data are combined with previous published data to derive a single rate equation that describes chlorite dissolution from 25 to 275°C from pH 3 to 10 (Lowson et al., 2007; Smith et al., 2013b). We focused on chlorite dissolution kinetics because, chlorite, an Mg- and Fe-bearing sheet silicate, is commonly found in many rock types as both a primary or secondary alteration mineral. This work builds on our previous study of chlorite dissolution for CO_2-EGS applications, by extending the solution pH to capture a wider range of geothermal conditions.

2. MATERIALS AND METHODS

The Mg-rich chlorite used was the same solid as in previous experiments (Smith et al., 2013b) was purchased from the Source Clays Repository (Purdue, Illinois) as “CCa-2” chlorite, collected from a locality in El Dorado County, California, and described previously by Post and Plummer, 1972. The bulk specimen was first crushed to pea-size and then mechanically crushed by micro-milling, with the 150-250 um size fraction collected for use. Approximately 1 g of chlorite was used per experiment. As reported in Smith et al. (2013b), the sample was identified as clinochlore variety, with only trace rutile impurities noted with scanning electron microscopy and electron dispersive spectrometry. Molar mineral dissolution rates reported below were calculated from elemental release data using the stoichiometry determined by Smith et al. (2013b) of $(Mg_{4.29}Al_{1.48}Fe_{0.10})(Al_{1.22}Si_{2.78})O_{10}(OH)_8$. The initial surface area of the unreacted 150-250 um size fraction was measured by multi-point N_2-BET as 4.9 ±0.3 m^2/g, similar to that reported for the hand-crushed samples used in Smith et al. (2013b). Post-reaction sample surface areas were also measured from randomly selected experiments and are discussed below in section 3.4. This stoichiometry (specifically the low iron content) and surface area measurements differ from those

values reported for this mineral by the Clay Minerals Society, but they have both been independently verified by another research group (Black and Haese, 2014).

All experiments were performed in a background matrix of reagent-grade 0.05m NaCl and distilled deionized water initially purged with N_2 gas to remove atmospheric oxygen. Reagent-grade hydrochloric acid (HCl) and sodium hydroxide (NaOH) were commonly used to adjust the pH of individual solutions to desired levels. Sodium tetraborate ($Na_2B_4O_7$) was also used as a buffering agent in specific experiments. Total chloride (Cl^-) levels in the experimental solutions were maintained at a constant value of 0.05m, but sodium levels varied up to 0.075m as a result of buffers and/or pH adjustment by sodium hydroxide. Experimental solution compositions are listed individually in Table 1.

Titanium single-pass mixed-flow reactors (e.g., Dove and Crerar, 1990) were used to conduct chlorite dissolution experiments over a temperature range of 100-275 C and a pH range of 5-10 at far-from-equilibrium conditions. A schematic of the experimental set-up may be found in Figure 1 of Smith et al. (2013b). Room temperature NaCl solutions were pumped into the experimental reactors to pressurize the system, and then the reactor was brought to temperature over a period of several hours while influent solution continued to flow at a constant flowrate of 0.5 mL min^{-1}. We refer to time $t = 0$ in the discussion and figures below as the time when the reactor system achieved its target temperature. Influent solution was forced to flow upwards past chlorite grains held between fine titanium meshes in an isolated sample holder within the experimental reactor, ensuring continuously mixed conditions of solution-mineral contact. Reactor system pressures were maintained well above boiling point pressures by the use of a dome-loaded back-pressure regulator and nitrogen gas at the reactor outlet. All wetted reactor surfaces (including the pump and back-pressure regulator) were made of C-276 alloy, passivated grade-4 titanium, or PEEK. To conclude each experiment, the reactor heaters were turned off and the sample was removed from each reactor as soon as liquid temperatures decreased below 100 °C. Sample holders were dried overnight at 60 °C and chlorite solids were then removed and preserved. Each reactor and pump was cycled with a mildly acidic (pH 4) HCl solution and then at least 24 hours of distilled water rinsing between experiments, and reactor parts were periodically boiled in 8N nitric acid and re-passivated.

Fluid chemistry samples were collected directly downstream of the back-pressure regulator through a luer-lock port using 60-mL disposable syringes. Effluent samples were split into three aliquots for analysis: 15 mLs were filtered (0.2 um) and acidified for silicon, magnesium, aluminum, iron, calcium and other trace metal analysis by inductively-coupled plasma mass spectrometry (ICP-MS); 1 mL was filtered and diluted by 10x distilled water for ion chromatography (IC) to confirm consistent background sodium (Na^+) and chloride (Cl^-) solution concentrations; 3-5 mLs were reserved, unfiltered, for 21 °C pH measurement. The geochemical code EQ3/6 and the updated *data.shv* database (Wolery, 1992; Johnson et al., 1992) were used to calculate solution pH at experimental temperatures as well as mineral-specific fluid saturation indices. To avoid propagating large errors from IC measurements into the calculation of solution pH, each solution chemistry dataset was first charge-balanced (on chloride, Cl^-) at 21 °C using measured solution pH values, and then modeled at the experimental temperature for determination of *in situ* solution pH.

3. RESULTS AND DISCUSSIONS

In this section we derive chlorite dissolution rate equation from pH 3 – 10 and 25 to 275°C by combining experimental dissolution rates, as determined by silica concentrations measured from new high temperature experiments and previously published experiments (Black and Haese, 2014; Smith et al., 2013b; Lowson et al., 2007), as well as discuss possible implications of near-equilibrium conditions and the observed pH dependence of non-stoichiometric dissolution.

3.1 Derivation of kinetic rate equations

We derived chlorite dissolution rate from pH 3 – 10 and 25 – 275°C by combining experimentally derived dissolution rates from new high temperature experiments and previously published experiments (Smith et al., 2013b; Black and Haese, 2014; Lowson et al., 2007). As was the case in our past work, net chlorite dissolution rates from flow-through reactor experiments were determined from measured effluent compositions after steady-state conditions (with respect to silica and pH) were achieved. Figure 1 shows examples of typical changes in common chemical aqueous constituents over time. For experiments conducted at neutral to basic pH (Figure 1B), a longer timeframe was necessary to reach steady-state conditions compared to previous experiments performed under more acidic conditions which achieved steady-state levels within 48-72 hours (Figure 1A; Smith et al., 2013b).

After normalization to total chlorite surface area and stoichiometric corrections, these rate data can be used to derive a general rate equation of the form:

$$R = \left(\left[k_{acid} \times e^{\left(\frac{-E_{acid}}{R} \times \left(\frac{1}{T} - \frac{1}{298} \right) \right)} \times a_{H^+}^{n} \right] + \left[k_{neut} \times e^{\left(\frac{-E_{neut}}{R} \times \left(\frac{1}{T} - \frac{1}{298} \right) \right)} \right] \right) \times \Delta G_r \quad (1)$$

where k represents the reaction rate constants (25 °C) for specific rate mechanisms, E represents activation energy values, a_{H+} is the activity of hydrogen ion, n is an order of reaction term, R represents the gas constant, and ΔG_r is a free energy of reaction term. In this formulation, two mechanisms (*acid* and *neutral*) are used to describe the dependence of chlorite dissolution on pH and temperature. Rate equations of this form may also include a third base-catalyzed mechanism (see Palandri and Kharaka, 2004), but examination of our data and that from Lowson et al. (2007) does not support the need for a third mechanism (see Figure 2). One advantage of this formulation is its ease of implementation into existing reaction codes; however, alternative formulations could account for some systematic differences between observed and predicted rate values from equation (1) (discussed further in section 3.3).

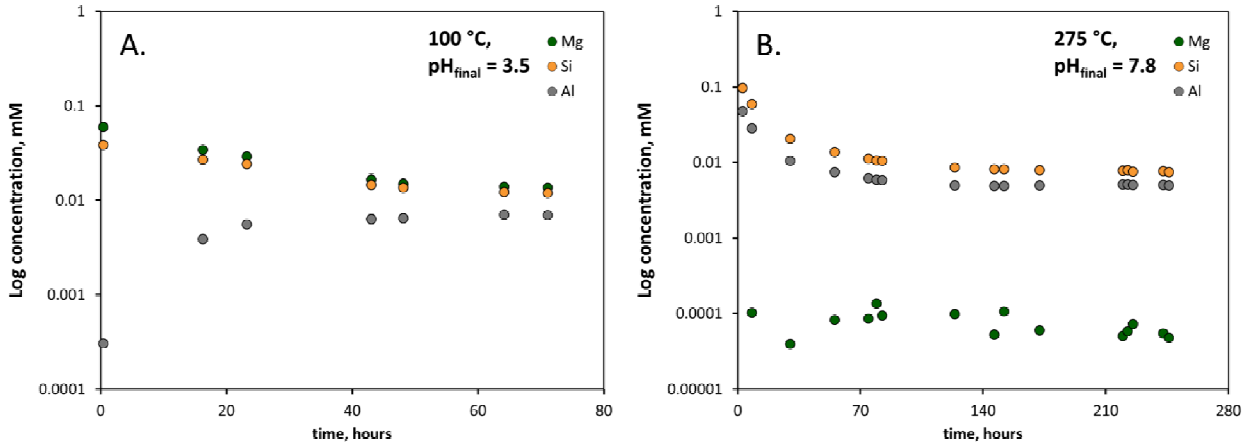

Figure 1: Typical experimental solution chemistry as a function of time for chlorite dissolution experiments conducted over a range of acid (e.g., A) and neutral to basic (e.g., B) pH conditions.

Figure 2 shows a selection of the experimental data used to derive the fit to equation (1) as a function pH and temperature. At a given temperature, dissolution rates decrease with pH in the acid pH region, achieving a minimum and*constant* value over neutral to alkaline pH levels. Our observations at high temperature are corroborated by rate versus pH trends observed in the lower-temperature (25-95 °C) data published by Lowson et al. (2007).

In a previous publication (Smith et al., 2013b), a subset of the data shown in Figure 2 were used to derive a kinetic dissolution rate equation for acidic conditions (pH<5) such as those encountered in a CO_2-enhanced geothermal system (CO_2-EGS). Based on that data treatment, which assumed an acid-catalyzed dissolution mechanism, chlorite dissolution was described with three parameters: n = 0.49; E_{acid} = 25.1 ($kJ\ mol^{-1}$); and log k_{acid}, 25 °C = -9.91 ($mol\ m^{-2}s^{-1}$). Inclusion of twenty new data points, collected under neutral and basic solution pH conditions over the same temperature range (100-275 °C) require a second mechanism of dissolution, insensitive to pH variations above a certain value (pH ≈ 6), to fit the data. The data and model fit shown in Figure 2 also include data published by Lowson et al. (2007) and Black and Haese (2014) which were collected with a similar single-pass flow-through setup at temperatures between 25 and 120 °C. Despite a number of differences in the experimental protocol (e.g., presence or lack of $CO_{2(aq)}$; presence of pH buffering agents) and chlorite mineral composition, good agreement was noted at 95 – 100 °C between our data and that of Lowson et al. (2007), with similar rate versus pH trends observed at all temperatures.

Optimized model parameters for n, k_{acid}, E_{acid}, k_{neut}, and E_{neut} (Equation 1) were derived by weighting all rate values (114 data points) equally and conducting a least-squares linear regression. Sensible starting values for acid and neutral activation energies were derived from graphical Arrhenius treatments of rates collected under similar pH conditions. The parameters were optimized by iteratively varying them (one at a time) to increase the regression coefficient, R^2, resulting in final parameter values of n = 0.56; activation energies E_{acid} = 24.9 and E_{neut} = 30.4 kJ mol^{-1}; and 25 °C log k_{acid} = -9.88 and log k_{neut} = -13.0 mol m^{-2} sec^{-1}. The final value of n is slightly larger than that predicted earlier in Smith et al. (2013b) but is well within range of other published estimates of this parameter (e.g., Lowson et al., 2005; Brandt et al., 2003; Gustaffson & Puidomenech, 2003). The values for the acid rate constant and activation energy are essentially unchanged from that reported in Smith et al (2013b), and the magnitude of the neutral rate constant at 25 °C is also nearly identical to that derived by Lowson et al. (2005) from lower-temperature dataset. While this rate formulation is a robust description of our and others' chlorite dissolution data, we recognize that other mechanisms and rate formulae may also describe the data and such investigation is the subject of ongoing work.

A global comparison of the experimentally measured and predicted rates is shown in Figure 3. The overall scatter of the data about the 1:1 (ideal) correlation line is greater than that attributable to uncertainty in surface area measurements (discussed further in section 3.4), which is not surprising given that three different datasets are represented. It is important to note that over a temperature span of 25-275 °C, the entire dissolution rate dataset spans a range of only 2.5-3 log units. This rather limited increase in chlorite dissolution rates with temperature suggests that chlorite may not be as reactive as previously indicated by simulations which incorporated rate equations with a much higher temperature dependence (Xu, 2012; Wolery and Carroll, 2010).

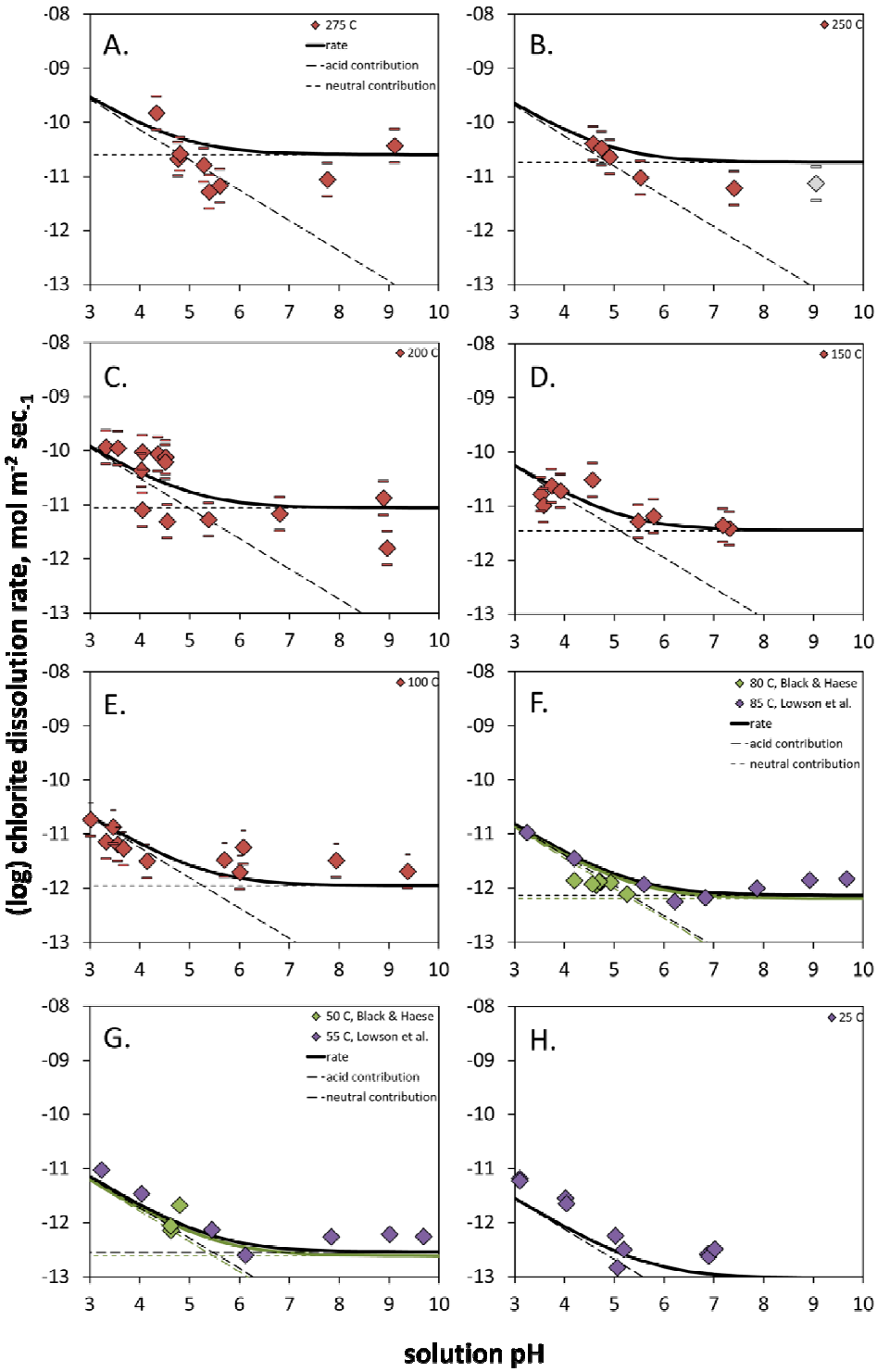

Figure 2: Chlorite dissolution rate versus solution pH at experimental temperatures from this study (red, all available data shown with bulk errors); Lowson et al. (2007, selected temperatures in purple); and Black & Haese (2014, selected temperatures in green). Heavy lines represent predicated rates at given temperatures from the proposed kinetic rate formulation discussed in section 3.1. Finer dashed lines represent individual acid and neutral contributions to the overall dissolution rate. The unfilled data point in plot (B) is shown for continuity but was not utilized for rate parameter determination due to its positive chlorite saturation index value (see section 2).

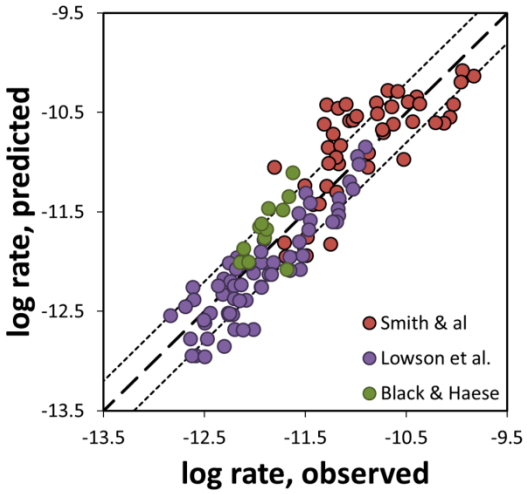

Figure 3: Observed versus predicted chlorite dissolution rates; data from this study and Smith et al. (2013b, in red); Lowson et al. (2007, in purple); and Black and Haese (2014, in green). The heavy dashed line indicates a 1:1 correlation between observed and predicted data. Fine dashed lines represent a bulk error contributed by uncertainty in surface area measurements, pre- and post-reaction (see section 3.4).

3.2 Effect of approach to equilibrium on rate magnitudes

Initial examination of chlorite rate data assumed that all values were measured under far-from-equilibrium conditions. However, closer inspection of the solution chemistry reveals that this may not be the case for experiments at more neutral to alkaline pH values, as shown in Figure 4 for data collected over a range of temperatures (25-275 °C). Saturation indices, defined as the logarithm of the ratio of the ion activity product, *IAP*, and the equilibrium constant for chlorite dissolution, K_{eq}, are shown to approach values of zero (indicating equilibrium) at solution pH values roughly greater than 7. We incorporate the approach to mineral equilibrium into equation (1) through the use of a Gibbs free energy of reaction term:

$$\Delta G_r = 1 - \frac{IAP}{K_{eq}} \tag{2}$$

where *IAP* is the ion activity product, and K_{eq} is the equilibrium constant for chlorite dissolution. The Gibbs free energy term allows mineral dissolution to slow as equilibrium is approached, effectively shutting down the chemical reactions. Those experiments with steady-state saturation indices greater than one (fourteen rate values from Lowson et al. (2007); one from this study, Figure 2B) were excluded from parameter optimization.

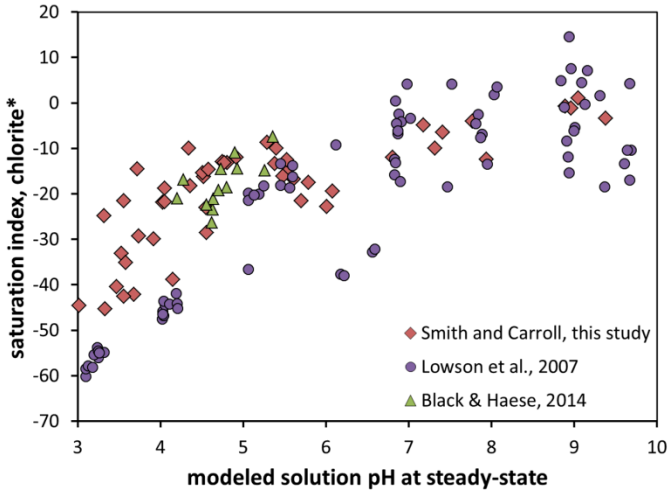

Figure 4: Modeled or reported fluid saturation index values (log IAP/K_{eq}) with respect to chlorite versus modeled stead-state solution pH (compensated for temperature). Note that this study and Black and Haese (2014) report values for *clinochlore-14A* from the *data.shv* database; Wolery (1992), while the remaining values are referenced to a *ripidolite* variety with log *K* values calculated by Lowson et al. (2007)

3.3 Stoichiometry of chlorite dissolution

Figure 5 plots the ratios of aqueous Mg/Si, Al/Si, and Fe/Si, where the dashed lines indicate stoichiometric dissolution as measured by equivalent concentrations in solution and chlorite mineral. Rate values shown in Figure 2 are derived from Si concentrations rather than Mg or Al (also major constituents of this chlorite variety), because neither magnesium nor aluminum displayed consistently stoichiometric release rates over a pH range of 3 to 10. Iron is a minor constituent in the variety of chlorite used in our experiments and shows complex dissolution trends when Fe/Si is plotted against pH. These trends are likely to be an artifact of the experimental system, because blank (mineral-free) experiments at similarly elevated temperatures revealed background iron contributions from the metal reactor and other pressure components.

The trends in Figures 5A and 5B suggest possible secondary precipitation of magnesium-bearing solids at pH > 5.5 and of aluminum-bearing solids at pH < 6-7. For experiments with low steady-state Al:Si ratios (generally, but not always, those conducted under low-pH conditions), diaspore, boehmite, and gibbsite were the most common mineral phases with modeled saturation indices indicating near-equilibrium or supersaturation. Saturation indices for brucite and chrysotile remained undersaturated but approached equilibrium under high-pH experimental conditions where some low Mg:Si ratios were noted. While powder X-ray diffraction did not yield evidence of secondary precipitates, a technique such as high-resolution transmission electron microscopy (TEM) is needed to detect small quantities of these potential mineral phases. The presence of chrysotile, a magnesian sheet silicate, or a similar Mg-silicate phase, is most intriguing as it could account for both lowered Mg:Si ratios and low overall silica concentrations (leading to low calculated dissolution rates) at higher pH values. To date we have obtained no evidence for this or any other secondary precipitate. However, the trends in Figures 5A and 5B, as well as the observation of slightly larger residual errors between observed and predicted rate values at the lowest and highest pH conditions, argues for consideration of the data with an alternative rate formulation that incorporates the effects of magnesium and aluminum release on silica-derived dissolution rates. The development of such a formulation is the subject of current work.

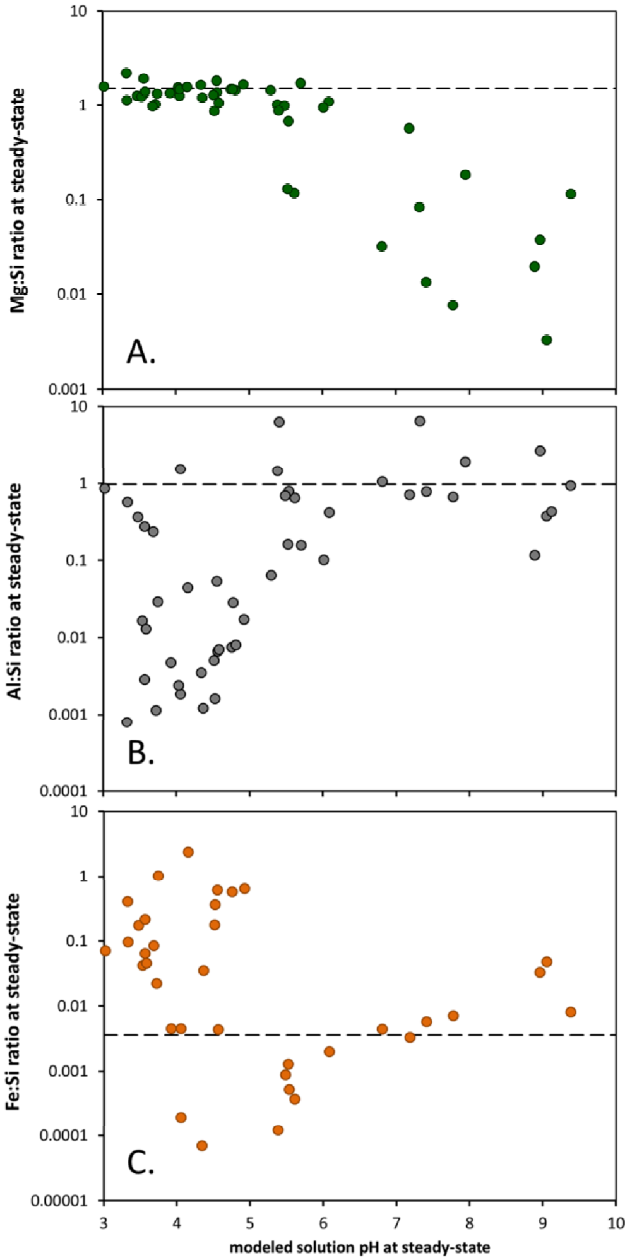

Figure 5: Ratios of steady-state release rates of A) magnesium:silica, B) aluminum:silica, and C) iron:silica versus modeled steady-state solution pH (compensated for temperature). Dashed horizontal lines represent the initial ratios at which these elements are present in the unreacted chlorite material.

3.4 Changes in reactive surface area

Reacted chlorite grains from neutral and basic solution pH experiments measured in this reporting period displayed surface area values that were about 2 times smaller than the initial unreacted chlorite. Multi-point N_2-BET measurements of different batches of unreacted micro-mill-ground "CCa-2" chlorite grains produced a surface area estimate of 4.9 ±0.3 m^2 g^{-1}, very similar to the estimate of 5.1 ±0.4 m^2 g^{-1} for the hand-crushed "CCa-2" chlorite (pre- and post-reaction) used in Smith et al. (2013b). After reaction for 80-240 hours in solutions of pH ≥5.5, surface area estimates of nine randomly selected chlorite samples had decreased by approximately 50%, to values of 2.3-2.6 m^2 g^{-1}. One possible explanation for the lower surface areas could be the dissolution of fines from the longer experimental durations of the neutral and alkaline experiments. This uncertainty in true reactive surface area (at steady-state times) causes a discrepancy in calculated surface area-normalized dissolution rates of ~0.3 log units. This difference is generally larger than that induced by other experimental factors (e.g., analytical chemistry methods, gravimetrically measured flowrates, sample collection durations), but is on the order of differences in individual rates calculated from replicate experiments. For the purposes of calculating surface-area normalized dissolution rates for the new data (i.e., neutral or alkaline data not reported previously in Smith et al. (2013b)), we chose to use the post-reaction measured surface area values (2.4 ±0.2 m^2 g^{-1}), because they are indicative of the later time conditions during the steady-state periods coinciding with the silica solution chemistry also used in rate derivation.

4. CONCLUSIONS AND IMPLICATIONS FOR EGS

The objective of this suite of experiments was to develop a useful kinetic dissolution expression for chlorite that would be applicable over a wide range of solution pH and temperature conditions representative of subsurface conditions in both natural and enhanced/engineered geothermal reservoirs. One possible rate equation is dependent on both pH and temperature, utilizing two specific dissolution mechanisms (an "acid" and a "neutral" mechanism), and was derived from data collected at LLNL and available published data from two other research groups (Lowson et al., 2007; Black and Haese, 2014). The form of this rate equation (equation 1) should be easy to incorporate into most existing reactive transport codes for use in prediction of rock-water interactions in EGS systems.

Specifically, we find that the dissolution of chlorite, a sheet-silicate, is relatively slow at elevated temperatures (100-275 °C), compared to other framework silicate minerals for which higher-temperature kinetic data are available (e.g., quartz and feldspars; see Palandri and Kharaka, 2004). This finding is in conflict with previously reported high activation energies (derived from a study by Ross, 1967) for chlorite based on extrapolation of low-temperature experimental data to higher temperatures. Additionally, we note that the observed dissolution of chlorite does not increase under alkaline conditions, as has been noted for other minerals, but rather remains at the same level as that noted for neutral conditions, with only a weak dependence on temperature.

Future work includes similar rate measurements and the derivation of useful rate equations for illite, smectite, biotite, and muscovite over pH ranges of 3 to 10 and temperatures of 100 to 275 °C. Useful and accurate descriptions of geochemical alteration, along with changing stress fields, mass transport and heat transfer, must be incorporated into computational models to optimize geothermal energy production for EGS systems. The resulting mineral rate equation described here can be directly incorporated in modeling efforts to better assess the impacts of geochemical alteration on long-term fracture permeability for EGS systems.

ACKNOWLEDGMENTS

We acknowledge support of this research through the U.S. Department of Energy, Geothermal Technologies Program. We also wish to thank LLNL personnel Victoria Gennetti and Rachel Lindvall (ICP-MS), as well as James Begg and Mavrik Zavarin (N_2-BET). This work was performed under the auspices of the U.S. Department of Energy by Lawrence Livermore National Laboratory under contract DE-AC52-07NA27344. LLNL–CONF-649929.

REFERENCES

Black, J.R., and Haese, R.R.: Chlorite dissolution rates under CO_2 saturated conditions from 50 to 120 °C and 120 to 200bar CO_2, *Geochimica et Cosmochimica Acta*, **125**, (2014), 225-240. 10.1016/j.gca.2013.10.021.

Brandt, F., Bosbach, D., Krawczyk-Bärsch, R., Arnold, T., and Bernhard, G.: Chlorite dissolution in the acid pH range: A combined microscopic and macroscopic approach, *Geochimica et Cosmochimica Acta*, **67**, (2005), 1451-1461. 10.1016/S0016-7037(02)01293-O.

Cama, J., Ganor J., Ayora, C., and Lasaga, C.A.: (2000) Smectite dissolution kinetics at 80°C and pH 8.8, *Geochimica et Cosmochimica Acta*, **64**, (2000) 2701-2717. 10.1013/S0016-7037(00)00378-1.

Carlson, S.R., Roberts J.J., Detwiler R.L., Viani B.E., and Roberts, S.K.: Fracture permeability evolution in Desert Peak Quartz Monzonite, *GRC Transactions*, **29**, (2005) 337-342.

Carroll, S.A., and Knauss, K.G.: Dependence of labradorite dissolution kinetics on $CO_{2(aq)}$, $Al_{(aq)}$, and temperature, *Chemical Geology*, **217**, (2005), 213-225. 10.1016/j.chemgeo.2004.12.008.

Dove, P.M., and Crerar, D.A.: Kinetics of quartz dissolution in electrolyte solutions using a hydrothermal mixed flow reactor, *Geochimica et Cosmochimica Acta*, **54**, (1990), 955-969. 10.1016/0016-7037(90)90431-J.

Gustafsson, A.B., and Puigdomenech, I.: The effect of pH on chlorite dissolution rates at 25 °C, *Materials Research Society Symposium Proceedings*, **757**, (2003), 649-655. 10.1557/PROC-757-II3.16

Johnson, J.W., Oelkers, E.H., and Helgeson, H.C.: SUPCRT92: a software package for calculating the standard molal thermodynamic properties of minerals, gases, aqueous species, and reactions from 1 to 5000 bar and 0 to 1000 C, *Computers and Geosciences*, 18, (**1992**), 899-947. 10.1016/0098-3004(92)90029-Q.

Köhler, S.J., Dufaud, F., and Oelkers, E.H.: An experimental study of illite dissolution kinetics as a function of pH from 1.4 to 12.4 and temperature from 5 to 50°C, *Geochimica et Cosmochimica Acta*, **67**, (2003), 3583-3594. 10.1016/S0016-7037(3)00163-7.

Lowson, R.T., Comarmond, M.-C.J., Rajaratnam, G., and Brown, P.L.: The kinetics of the dissolution of chlorite as a function of pH and at 25°C, *Geochimica et Cosmochimica Acta*, **69**, (2005), 1687-1699. 10.1016/j.gca.2004.09.028.

Lowson, R.T., Brown, P.L., Comarmond, M.-C.J., and Rajaratnam, G.: The kinetics of chlorite dissolution, *Geochimica et Cosmochimica Acta*, **71**, (2007), 1431-1447. 10.1016/j.gca.2006.12.008.

Palandri J., and Kharaka, Y.K.: A compilation of rate parameters of water-mineral interaction kinetics for application to geochemical modeling, U.S. Geological Survey Open File Report 2004-1068, (2004), 70p.

Polak, A., Elsworth, D., Yasuhara, H., Grader, A.S., and Halleck, P.M.: Permeability reduction of a natural reaction under net dissolution by hydrothermal fluids, *Geophysical Research Letters*, **30**, (2003), 2020. 10.1029/2003GL017575.

Post, J.L., and Plummer, C.C.: The chlorite series of Flagstaff Hill area, California: A preliminary investigation, *Clays & Clay Minerals*, **20**, (1972), 271-283. 10.1346/CCMN.1972.0200504.

Ross, G.J.: Kinetics of acid dissolution of an orthosilicate mineral, *Canadian Journal of Chemistry*, **45**, (1967), 3031-3034. 10.1139/v67-491.

Smith, M.M., Walsh, S.D.C., McNab, W.W., and Carroll, S.A.: Experimental investigation of brine-CO_2 flow through a natural fracture: Permeability increases with concurrent dissolution/reprecipitation reactions, *Proceedings*, 38th Workshop on Geothermal Reservoir Engineering, Stanford University, Stanford, CA (2013a).

Smith, M.M., Wolery, T.J., and Carroll, S.A.: Kinetics of chlorite dissolution at elevated temperatures and CO_2 conditions, *Chemical Geology*, 347, (2013b), 1-8. 10.1016/jchemgeo.2013.02.017.

Viani, B.E., Roberts, J.J., Detwiler, R.L., Roberts, S.K., and Carlson, S.R.: Simulating injectate/rock chemical interaction in fractured Desert Peak Quartz Monzonite, *GRC Transactions*, 29, (2005), 425-430.

Wolery, T.J.: EQ3/6, a software package for geochemical modeling of aqueous systems, Lawrence Livermore National Laboratory Report UCRL MA-110662-PT-1, (1992).

Wolery, T.J., and Carroll, S.A.: CO_2-rock interactions in EGS-CO_2: New Zealand TVZ geothermal systems as a natural analog, *GRC Transactions*, **34**, (2010), 729-736.

Xu, T.: Mineral carbonation in a CO_2-EGS geothermal reservoir, *Proceedings*, 37th Workshop on Geothermal Reservoir Engineering, Stanford University, Stanford, CA (2012).

Yasuhara, H., Polak, A., Mitani, Y., Grader, A.S., Halleck, P.M., and Elsworth, D.: Evolution of fracture permeability through fluid-rock reaction under hydrothermal conditions, *Earth and Planetary Science Letters*, **244**, (2006), 186-2000. 10.1016/j.epsl.2006.01.046.

Yasuhara, H., Kinoshita, N., Ohfuji, H., Lee, D.S., Nakashima, S., and Kishida, K.: Temporal alteration of fracture permeability in granite under hydrothermal conditions and its interpretation by coupled chemo-mechanical model, *Applied Geochemistry*, **26**, (2011), 2074-2088. 10.1016/j.apgeochem.2011.07.005.

Yasuhara, H., and Elsworth, D.: Compaction of a rock fracture moderated by competing roles of stress corrosion and pressure solution, *Pure and Applied Geophysics*, **165**, (2008), 1289-1306. 10.1007/s00024-008-0356-2.